Geodesic Patterns

Helmut Pottmann KAUST, TU Wien
Qixing Huang Stanford University
Bailin Deng TU Wien
Alexander Schiftner Evolute GmbH, TU Wien
Martin Kilian TU Wien
Leonidas Guibas Stanford University
Johannes Wallner TU Graz, TU Wien

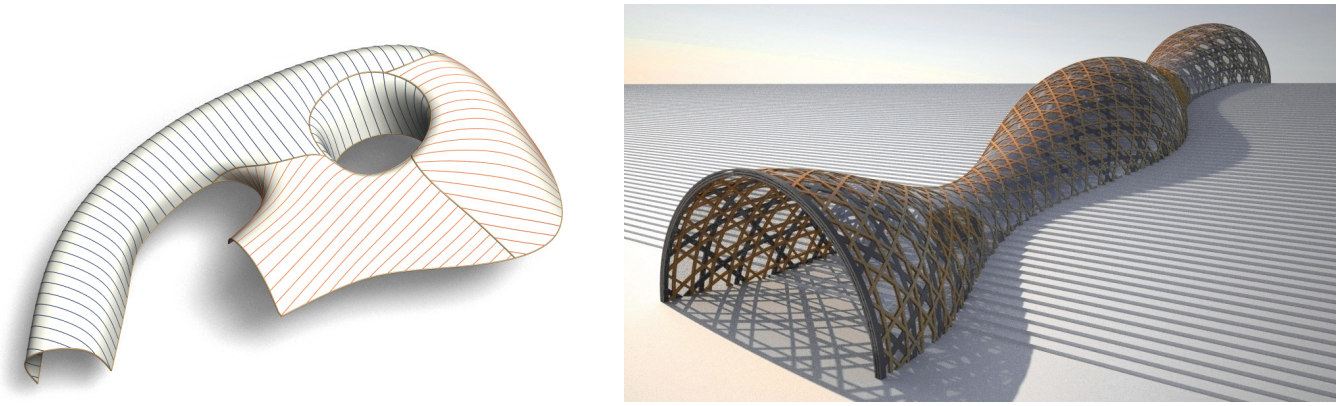

Figure 1: *Geodesic patterns on freeform surfaces*. Left: For the cladding of a surface by wooden panels bendable only about their weak axis, we perform segmentation into parts which can be covered by geodesic strips of roughly constant width. Right: A timber construction derived from a hexagonal geodesic web has good manufacturing and statics properties.

Abstract

Geodesic curves in surfaces are not only minimizers of distance, but they are also the curves of zero geodesic (sideways) curvature. It turns out that this property makes *patterns of geodesics* the basic geometric entity when dealing with the cladding of a freeform surface with wooden panels which do not bend sideways. Likewise a geodesic is the favored shape of timber support elements in freeform architecture, for reasons of manufacturing and statics. Both problem areas are fundamental in freeform architecture, but so far only experimental solutions have been available. This paper provides a systematic treatment and shows how to design geodesic patterns in different ways: The evolution of geodesic curves is good for local studies and simple patterns; the level set formulation can deal with the global layout of multiple patterns of geodesics; finally geodesic vector fields allow us to interactively model geodesic patterns and perform surface segmentation into panelizable parts.

CR Categories: I.3.5 [Computer Graphics]: Computational Geometry and Object Modeling—Geometric algorithms, languages, and systems; I.3.5 [Computer Graphics]: Computational Geometry and Object Modeling—Curve, surface, solid, and object representations

Keywords: computational differential geometry, architectural geometry, geometry of webs, timber rib shell, cladding, freeform surface, pattern, geodesic, Jacobi field.

ACM Reference Format
Pottmann, H., Huang, Q., Schiftner, A., Kilian, M., Guibas, L., Wallner, J. 2010. Geodesic Patterns. *ACM Trans. Graph. 29*, 4, Article 43 (July 2010), 10 pages. DOI = 10.1145/1778765.1778780 http://doi.acm.org/10.1145/1778765.1778780.

1 Introduction

In recent years it has become apparent that methods from Geometric Computing bear a great potential to advance the field of freeform architecture. This fact has created the new research area *architectural geometry*, which draws from various branches of geometry and which is motivated by problems originating in architectural design and engineering – see for instance the proceedings volume [Pottmann et al. 2008a]. The topics studied in the present paper belong to this line of research. They have as a common theme the *design of a pattern of geodesics on a freeform surface*.

One problem concerns the cladding of a general double curved surface with wooden panels. Such claddings will be mainly applied to interior spaces (see Fig. 2). Even if the material may be different from wood, the panels are assumed to be close to developable and their development should fit well into a rectangle whose length is much larger than its width. Hence, each panel should follow a *geodesic curve*. The cladding problem can be approached in an experimental way as illustrated by Fig. 2. Computationally it means decomposing a given surface into regions, each of which can be covered by a sequence of nearly equidistant geodesic curves (see Fig. 1).

Other applications of geodesic patterns lie in wooden constructions where the geodesics are used for the *supporting structure of a curved shell*. Extending pioneering technologies by J. Natterer [2002], ongoing research at the EPF Lausanne aims at the design of freeform timber rib shells, which are composed of a grid of geodesic curves (see Fig. 3). Other innovative timber constructions, as seen in recent projects by Shigeru Ban (Fig. 4), would also benefit from an efficient computational approach to the layout of geodesic patterns on surfaces. One reason why geodesic curves are a preferred shape is statics: Geodesics – being minimizers of distance – are the equilibrium shapes of elastic curves constrained to the surface. Another reason is the manufacturing of laminated beams, which are much easier to make if the individual boards can simply be twisted and bent and along the weak axis [Pirazzi and Weinand 2006].

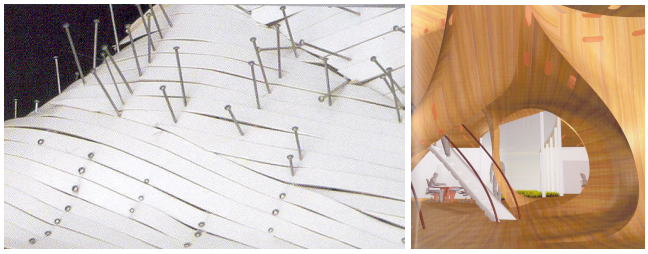

Figure 2: Experimental cladding using paper strips (left) results in an office space design by NOX Architects [Spuybroek 2004].

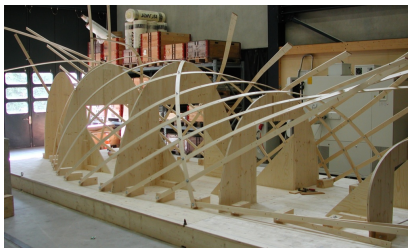

Figure 3: Assembling screw-laminated beams for a timber rib shell prototype based on a 2-pattern of geodesics. Image courtesy IBOIS, the timber construction lab at EPF Lausanne.

Related work. Let us briefly address the literature in geometric computing, as far as it is obviously related to our problem formulation. We will later encounter more connections to previous work.

A geodesic curve g is a locally shortest path on a surface S. The computation of geodesics is a classical topic: For smooth surfaces, pursuing a geodesic curve emanating from a point with a given tangent vector is equivalent to solving an initial value problem for a 2nd order ODE, while the boundary value problem (connecting two points on a surface by a geodesic path $\mathbf{c}(t)$) can be converted into the constrained minimization of the quadratic energy $\int \|\dot{\mathbf{c}}\|^2$ [do Carmo 1976]. For triangle meshes, shortest polylines cross edges at equal angles, and ambiguities at vertices may be resolved by the concept of "straightest geodesics" [Polthier and Schmies 1998]. Finding the truly shortest geodesic paths requires the computation of distance fields, for which several efficient algorithms have been developed, see for instance [Chen and Han 1996] or [Kimmel and Sethian 1998].

Early research on the cladding of freeform surfaces with developable panels evolved from the architecture of F. Gehry [Shelden 2002]. One contribution to the present cladding problem is provided by the *geodesic strip models* of Pottmann et al. [2008b]. This name is used for continuous surfaces composed of developable strips which have nearly straight development. One can view them as semi-discrete versions of smooth families of geodesics on a smooth surface. In general, several geodesic strip models with different directions are required to cover a freeform surface (see Fig. 2). The choice of these directions and the initialization of the optimization in [Pottmann et al. 2008b] has not been systematically investigated so far.

Figure 4: Timber construction for the Yeoju Golf Club by Shigeru Ban; CAD/CAM by *designtoproduction*. The beams are no geodesics and manufacturing thus requires CNC machining. We address the design of 3-patterns of geodesics and so contribute to their simplified manufacturing.

Our approach to geodesic patterns is closely related to classical results on the geometry of webs which was developed mainly by W. Blaschke and his school. We refer to the survey article [Chern 1982] and the monograph [Blaschke and Bol 1938].

Contributions and overview. Inspired by practical problems in architecture, we study *geodesic N-patterns* on surfaces. These are formed by N discrete families of geodesics which are subject to additional constraints arising from the specific application. We put particular emphasis on the cases $N = 1$ (Fig. 2), $N = 2$ (Fig. 3) and $N = 3$ (Fig. 4). The overall goal is to provide an efficient computational framework to support the user's navigation through design space. Our results include:

- ways to control the strip width variation in a geodesic 1-pattern based on geometric concepts such as Jacobi fields and striction curves (Sec. 2);
- two computational approaches for designing geodesic 1-patterns, namely an evolution algorithm guided by Jacobi fields (Sec. 3) and a level set approach which is also used for the design of general N-patterns (Sec. 4);
- the design of geodesic webs (special 3-patterns and 4-patterns) and the extraction of further patterns from such webs, for instance in the style of Islamic art (Sec. 5);
- a user-friendly design tool for the solution of the cladding problem which results in an aesthetically pleasing segmentation of the design surface into regions covered by geodesic 1-patterns. This tool is based on the concept of piecewise-geodesic vector fields (Sec. 6).

Each of these approaches solves different instances of the problem of covering a surface with geodesic curves.

2 Distances between geodesics

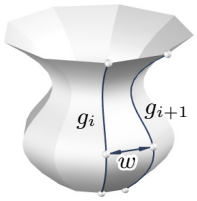

In this section, we discuss general sequences (*1-patterns*) $\{g_i\}$ of successive geodesic lines in a surface and the distances between them. It is not usually possible to express by formulas such a distance – say between the geodesic curve g_i and its neighbor g_{i+1}. Not even an exact definition of such a distance is straightforward. Only in some highly symmetric cases, like evenly distributed meridian curves of a rotational surface (see the figure) the measurement of distance is elementary. However, a first order approximation of that distance is well known: Start at time $t = 0$ with a geodesic curve $g(s)$, which is parametrized by arc length s, and let it move smoothly with time. A snapshot at time $t = \varepsilon$ yields a geodesic g^+ near g (see Fig. 5):

$$g^+(s) = g(s) + \varepsilon \mathbf{v}(s) + \varepsilon^2(\dots).$$

The derivative vector field $\mathbf{v}$ is called a *Jacobi field*. It is known that without loss of generality we may assume that it is orthogonal to the curve $g(s)$, and it is expressed in terms of the geodesic's

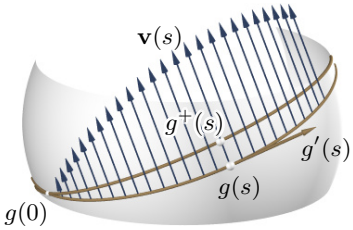

Figure 5: A geodesic $g(s)$ with Jacobi field $\mathbf{v}(s)$, and a neighboring geodesic $g^+(s)$ which is at distance $\approx \varepsilon\|\mathbf{v}(s)\|$. The parameter s is the arc length along the geodesic g, and $\mathbf{v}$ obeys the Jacobi differential equation (1). Here $\mathbf{v}(0) = 0$.

tangent vector g' as

$$\mathbf{v}(s) = w(s) \cdot R_{\pi/2}(g'(s)), \quad \text{where } w'' + Kw = 0. \qquad (1)$$

Here R_α is the rotation by the angle α in the tangent plane of the surface, and K is the Gaussian curvature [do Carmo 1976].

Since distances between infinitesimally close geodesics are governed by (1), that equation also approximately governs the width of a strip bounded by two geodesic curves of small finite distance. Note that the Jacobi equation can also be used to fabricate surfaces of given Gaussian curvature, by gluing together strips of paper whose width obeys the Jacobi differential equation (see Fig. 6).

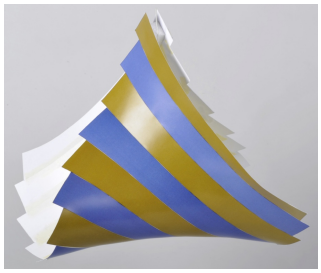

$$w(s) = \alpha \cosh(s\sqrt{|K|})$$

Figure 6: *Do it yourself K-surface*. We glue together strips whose width $w(s)$ fulfills the Jacobi equation for some constant value $K < 0$. This results in a surface of approximately constant Gaussian curvature.

A first design method for geodesic 1-patterns. For the design of a geodesic 1-pattern $\{g_i\}$ it is important to control the positions of points at which the distance of the curve g_{i+1} from the curve g_i assumes a minimum or maximum. It turns out that it is not difficult to design 1-patterns of geodesics where the locus of these points is prescribed. The Jacobi relation (1) is the key to understanding the local behavior of the strip width.

Assuming $w > 0$, we have $w'' < 0$ whenever the Gaussian curvature is positive. Therefore in an area where $K > 0$, the strip width can have only maxima. If the Gaussian curvature is negative, then the strip width can have only local minima. The case of *constant* strip width is only possible if $K = 0$, which means developable surfaces.

Setting aside the special case of developable surfaces, we get a picture of the locus of extremal strip width by first looking at the case of a smooth family $\{g_t\}$ of curves on a surface. The *striction curve* $\mathbf{s}$ is the locus of extremal width of the infinitesimal strips defined by two neighboring curves of the family (generically $\mathbf{s}$ is curve-like, but it may also degenerate). H. R. Müller [1941] showed the following: If the curves g_t are geodesics, their initial tangent vectors are geodesically parallel along $\mathbf{s}$. Conversely, if we compute a geodesically parallel vector field $\mathbf{v}(t)$ along a curve $\mathbf{s}(t)$ and then trace the geodesics with start at points $\mathbf{s}(t)$ with initial tangent vector $\mathbf{v}(t)$, then $\mathbf{s}$ is (part of) the striction curve of this family of geodesics.

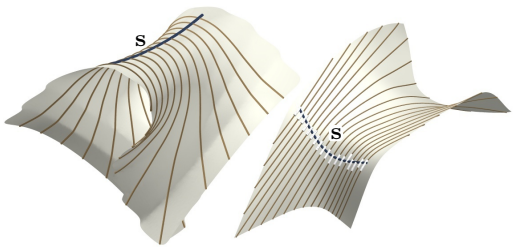

Figure 7: The striction curve $\mathbf{s}$ of a geodesic 1-pattern. If the initial tangent vectors of geodesics constitute a *geodesically parallel vector field* along $\mathbf{s}$, then extremal distances between successive curves occur near $\mathbf{s}$. *Left:* the piecewise-developable surface of Fig. 6. *Right:* The areas of extremal distance of a geodesic curve from its neighbors are indicated by white color. This surface is taken from the *Cagliari museum project* by Zaha Hadid architects.

Knowing this, the design of geodesic patterns with prescribed striction curve $\mathbf{s}(t)$ is simple: Once the striction curve $\mathbf{s}$ is chosen, there is only one remaining degree of freedom in the choice of the parallel vector field. From this 1-parameter family of patterns we can take the one which best fits the design intent (see Fig. 7).

3 Geodesic 1-patterns by evolution

This section presents a strategy for the design and computation of geodesic 1-patterns on triangle meshes which represent general freeform surfaces. It is based on an evolution of curves, where the transfer from a current geodesic curve g to the next one (denoted by g^+) considers only the local neighborhood of g and can thus nicely be governed by Jacobi vector fields.

Solution of the Jacobi differential equation. The computation of all possible Jacobi vector fields $\mathbf{v}(s)$ orthogonal to a geodesic curve which is given by an arc length parametrization $g(s)$ $(0 \le s \le L)$ is easy. We only have to compute the function $w(s)$ which gives the length of the Jacobi field, and which satisfies the differential equation $w'' + Kw = 0$. This is a linear ODE with coefficient function $K = K(g(s))$. Any solution $w(s)$ is a linear combination

$$w(s) = \lambda_1 w^{(1)}(s) + \lambda_2 w^{(2)}(s)$$

of two linearly independent fundamental solutions $w^{(1)}$ and $w^{(2)}$.

We have implemented the solution of the Jacobi differential equation as follows: The geodesic under consideration is represented as a polyline $p_0, p_1, \ldots, p_M$ with edge lengths $L_i = \|p_{i+1} - p_i\|$. The unknown function w is given by its values $w_i = w(p_i)$ in the vertices p_i. Now the second derivative w'' is approximated by

$$w_i'' \approx \frac{2}{L_{i-1} + L_i}\Big(\frac{1}{L_i}(w_{i+1} - w_i) - \frac{1}{L_{i-1}}(w_i - w_{i-1})\Big).$$

In this way the Jacobi equation turns into a sparse linear system, involving $M-1$ equations for $w_1'', \ldots, w_{M-1}''$ in $M+1$ unknowns $w_0, \ldots, w_M$. If we prescribe the pair (w_0, w_1) of values, the system reduces to a triangular one. For the computation of the fundamental solutions $w^{(1)}$ and $w^{(2)}$ we simply choose these pairs to be $(0,1)$ and $(1,0)$, respectively.

Selecting a Jacobi field. The selection of the Jacobi field which is to guide the next geodesic g^+ depends on the design intent. If we are interested in constant strip width $w \approx W = \text{const.}$, we compute λ_1, λ_2 by minimizing

$$F_w = \int_{[0,L]} (\lambda_1 w^{(1)}(s) + \lambda_2 w^{(2)}(s) - W)^2 ds, \qquad (2)$$

which amounts to a linear 2×2 system. Since we have only two degrees of freedom, we cannot expect $\lambda_1 w^{(1)}(s) + \lambda_2 w^{(2)}(s) \approx$ const. in all cases. It is therefore advisable to check afterwards if we really have $w(s) \in [W - \varepsilon_1, W + \varepsilon_2]$, for certain pre-assigned tolerances $\varepsilon_1, \varepsilon_2$. See Figures 8a,d for an example.

Replacing the constant W by a prescribed function $W(s)$ is computationally the same, but opens up many possibilities: The decomposition of a freeform surface into strips might require a denser sampling if the curvature across the strips is high. We therefore guide strip width by minimizing F_w with $W(s) = \phi(\kappa_n(s))$, where ϕ is a strictly decreasing function and κ_n is the surface's normal curvature in the direction orthogonal to the given geodesic. For an example, see Fig. 8b. Prescribed patterns of geodesic curves can be achieved by appropriate choices of $W(s)$ (see Fig. 8c).

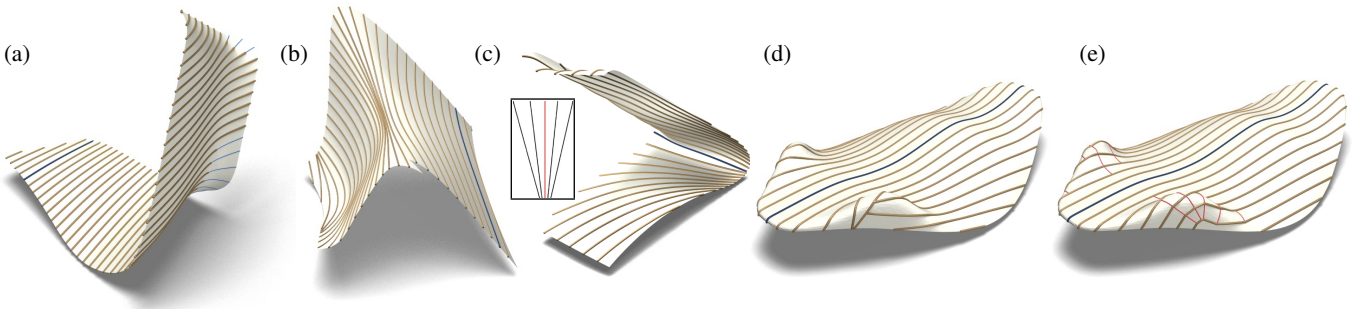

Figure 8: *Evolution of geodesics*, starting from a source curve (dark blue). (a) Regular equidistant evolution. Thin blue pieces of curves show where the distance constraint is violated. (b) Aesthetic reasons might require denser strips if the normal curvature across the strip is high. (c) Pattern transfer. The small image shows some intended width functions $W(s)$. (d) Because of positive Gaussian curvature, in some areas evolution is possible only if we allow intersections of adjacent geodesics. (e) Evolution of the same geodesic curve as in (d), but by introducing breakpoints if the strip width deviates too much from a constant value. The breakpoints are guided along the red curves.

Computing the next geodesic. The function $w(s)$ computed above approximately describes the distance between the geodesic curve g and the 'next geodesic' g^+. We could now find g^+ by simply moving the endpoints $g(0), g(L)$ sideways by the amounts $w(0)$, $w(L)$, respectively, and connecting them by a geodesic g^+. The following method takes more information into account:

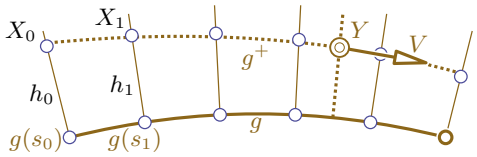

We sample the original geodesic at parameter values $s_i = \frac{i}{N}L$ $(i = 0, \ldots, N)$ and move the points $g(s_i)$ sideways on geodesics h_i orthogonal to g. This results in points X_i. The next geodesic g^+ is represented by a point Y which slides along a curve orthogonal to the current geodesic g and by an initial tangent vector V. These two degrees of freedom are determined such that $\sum_i \text{dist}(g^+ \cap h_i, X_i)^2$ (each distance measured along h_i) becomes minimal. Being close to the solution already, this can be done by a Levenberg-Marquardt method which avoids second derivatives.

Limitations of the evolution method. The method above which finds a smooth geodesic at a certain nonzero distance from a given one works only if one can find a width function w which solves the Jacobi equation and which has no zeros in the considered interval. It turns out that we can tell the existence of such 'useful' solutions simply by testing if the fundamental solution $w^{(1)}$ has another zero in the considered interval. The proposition below, proved in [do Carmo 1992], characterizes the two possible cases (good and bad) and sums up some of their geometric properties.

PROPOSITION 1. *Consider a geodesic curve $g(s)$, where $s \in [0, L]$ is an arc length parameter. Assume a fundamental solution $w^{(1)}(s)$ of the Jacobi equation with $w^{(1)}(0) = 0$. Then there are the following two cases:*

	case 1	*case 2*
# zeros of $w^{(1)}(s)$ for $0 < s \leq L$:	0	≥ 1
# zeros of any solution in the interval $[0, L]$:	≤ 1	≥ 1
existence of solution nonzero in $[0, L]$	*yes*	*no*
g locally minimizes distance of $g(0)$, $g(L)$	*yes*	*no*

The inequality $K(s) > (\pi/L)^2$ for $s \in [0, L]$ implies case 2. Analogously $K(s) < (\pi/L)^2$ implies case 1 (surely true if $K \leq 0$).

If the geodesic curve under consideration is a case 2 curve we have two choices (illustrated by Figures 8d,e): Either to put up with the fact that we cannot have a proper non-intersecting next geodesic, or to consider *broken geodesics*, which are the topic of the following paragraph.

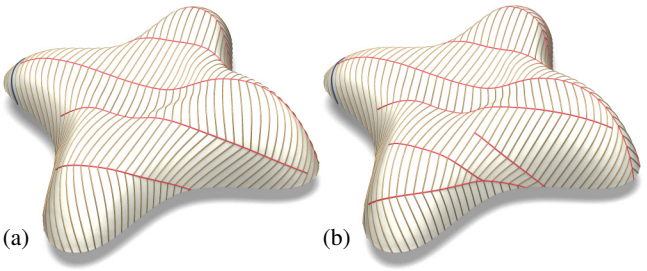

Figure 9: Evolution of a 1-pattern of broken geodesics, which starts with an unbroken one (blue, at extreme left). The threshold for the introduction of breakpoints in (a) and (b) is that the strip width deviates more than 7.5% or 5%, resp., from the desired value (this surface is taken from the top of the *Lilium tower*, Warsaw, by Zaha Hadid Architects).

Extension to broken geodesics Evolving a geodesic curve into a 1-pattern frequently runs into obstacles, due to the few degrees of freedom available. We therefore relax the geodesic condition and consider *broken geodesic curves*. Such a curve g consists of geodesic arcs g_i defined in arbitrary subintervals $[s_i, s_{i+1}]$. These arcs fit together at points $P_i = g_{i-1}(s_i) = g_i(s_i) = g(s_i)$. We evolve each arc g_i separately, with its own width function $w_i(s)$ which satisfies the Jacobi equation. Obviously, the single functions w_i are not independent. We draw the following picture:

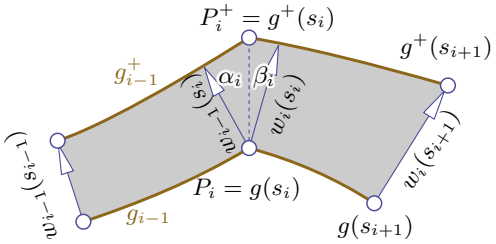

With the angles α_i, β_i between curve normals and the line connecting breakpoints, we read off the approximate relation

$$\frac{w_{i-1}(s_i)}{\cos\alpha_i} = \frac{w_i(s_i)}{\cos\beta_i}, \tag{3}$$

which assumes that the derivatives of w_{i-1}, w_i are small. We can now find the single width functions w_i by first choosing the di-

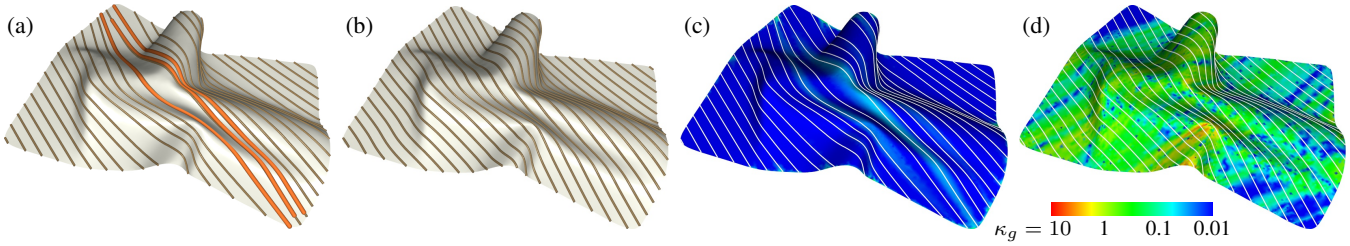

Figure 10: 1-patterns of geodesic curves which are found as level sets of a real-valued function defined on the surface. (a) Optimization with a low weight on F_w yields almost true geodesics. Three geodesics are shown in orange for comparison. (b) A higher weight on F_w generates strips of even width, but lets level sets deviate from true geodesics and creates higher geodesic curvatures. (c) and (d): Deviation from the geodesic property for subfigures (a) and (b). We show the geodesic curvature κ_g on a logarithmic scale; bounding box diagonal equals 4.

rection of movement of the breakpoints, reading off the angles α_i, β_i, and subsequently minimizing the sum of all F_{w_i} as defined by (2) with (3) as side condition. The 'next' geodesics g_i^+ are subsequently fitted to the width functions in a manner similar to the computation of the next geodesic which is described above. With the path of breakpoints already prescribed, the number of degrees of freedom for the broken geodesic g^+ is the number of segments plus one.

In the examples of Figures 8e and 9 breakpoints are automatically inserted whenever a strip would violate the distance constraint, and the paths of breakpoints are guided such that they bisect the angle of their adjacent geodesic segments.

4 Geodesic *N*-patterns from level sets

The Jacobi field approach is well suited if, in a 1-pattern, we want to move from one geodesic to the next, in a way which allows us to control the distance between these two geodesics. For *global* tasks such as an optimal alignment of a 1-pattern of geodesics with a vector field, or design problems involving several 1-patterns, we prefer to represent the geodesics of a 1-pattern as selected level sets of a real valued function ϕ which is defined on the given surface S.

Geodesic level sets are not new, in fact they represent the main idea in the geodesic active contour method of Caselles et al. [1997]. The difference to our setting is that we consider global patterns of geodesics. For level set methods in general we refer to [Osher and Fedkiw 2002].

Geodesic curves are characterized by vanishing geodesic curvature κ_g [do Carmo 1976]. If a curve is given in implicit form as a level set $\phi = \text{const.}$, then its geodesic curvature can be computed by

$$\kappa_g = \operatorname{div}\Big(\frac{\nabla\phi}{\|\nabla\phi\|}\Big), \tag{4}$$

where div, ∇ are understood in the intrinsic geometry of S (see e.g. [do Carmo 1992], p. 142).

We implement construction of a function ϕ as follows. The surface S is represented by a triangle mesh (V, E, F). The function ϕ is determined by its values on vertices and is considered to be linear within each triangular face. The level sets under consideration are polylines on the mesh. The vector field $\nabla\phi$ is constant in each face. For any vector field X we evaluate $\operatorname{div}(X)$ at a vertex $\mathbf{v}$ by computing the flux of X through the boundary of $\mathbf{v}$'s intrinsic Voronoi cell, divided by the area of that cell.

For regularization, we wish to keep $\Delta\phi = \operatorname{div}(\nabla\phi)$ small. Further, applications might require the distance between level sets $\phi = c$ and $\phi = c + h$ to equal some value w; for that distance we have

$$w \approx h \,/\, \|\nabla\phi\|. \tag{5}$$

We thus optimize ϕ by solving a nonlinear least squares problem which is governed by a linear combination of three functionals: F_κ penalizes deviation from zero geodesic curvature, F_Δ is for smoothing/regularization, and F_w penalizes deviation from the desired strip width w. Definitions are:

$$\begin{aligned} F_\kappa &= \sum\nolimits_{\mathbf{v}\in V} \mathcal{A}(\mathbf{v})\big(\operatorname{div}\frac{\nabla\phi}{\|\nabla\phi\|}(\mathbf{v})\big)^2, \\ F_\Delta &= \operatorname{area}(S)\sum\nolimits_{\mathbf{v}\in V} \mathcal{A}(\mathbf{v})\Delta\phi(\mathbf{v})^2, \\ F_w &= \sum\nolimits_{f\in F} \operatorname{area}(f)\Big(\|\nabla\phi(f)\| - \frac{h}{w}\Big)^2. \end{aligned}$$

Here $\mathcal{A}(\mathbf{v})$ means the area of the Voronoi cell of $\mathbf{v}$. All three functionals are invariant w.r.t. scaling of the geometry. We therefore formulate our optimization as

$$F_\kappa + \lambda F_\Delta + \mu F_w \to \min. \tag{6}$$

We initialize optimization by a function which minimizes F_Δ alone, under the side condition of 3 arbitrary function values. Results of this method can be seen in Fig. 10. As is to be expected we cannot make make F_κ and F_w vanish at the same time: Only for developable surfaces ($K = 0$) the geodesic property is compatible with constant width between curves.

For an N-pattern of geodesics, each of the N families of curves involved is represented as level sets of a function ϕ_i ($i = 1, \ldots, N$). We now minimize the sum of the single target functions analogous to (6). We can also incorporate additional requirements, for instance constant intersection angle α between families i and j. To this end we augment the target functional by

$$\nu \cdot F_{\text{angle}} = \nu \sum_{f\in F} \frac{\operatorname{area}(f)}{\operatorname{area}(S)} \Big\langle \frac{\nabla\phi_i}{\|\nabla\phi_i\|}, R_{\frac{\pi}{2}-\alpha}\big(\frac{\nabla\phi_j}{\|\nabla\phi_j\|}\big)\Big\rangle^2.$$

Here $R_{\frac{\pi}{2}-\alpha}$ means a rotation by the angle $\frac{\pi}{2} - \alpha$ in the respective face; ν is the weight given to F_{angle}. For an example see Fig. 16.

The level set approach is an integral part of the examples and images in Sections 5 and 6.

Remark 1. Our level set approach works only for simply connected surfaces. It is possible to extend it to arbitrary surfaces by using branched coverings, such as in [Kälberer et al. 2007].

Implementation details. To compute the function ϕ which minimizes the combined functional (6), we employ a classical Gauss-Newton method with line search for optimization [Madsen et al. 2004]. The variables of this optimization are the values of the unknown function ϕ on the vertices of a mesh. All required first order derivatives are calculated analytically (i.e., are not approximated).

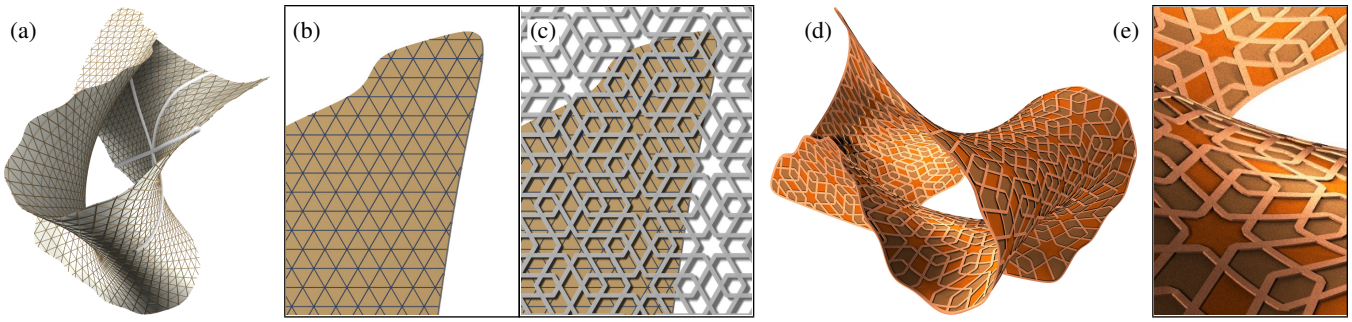

Figure 11: *A hexagonal web of geodesics* imposed on the surface of Fig. 6. The level sets of functions ϕ_1, ϕ_2, ϕ_3 are geodesics, if they obey $\mathrm{div}(\nabla\phi_i/\|\nabla\phi_i\|) = 0$. If they also obey $\phi_1 + \phi_2 + \phi_3 = 0$, they form a hexagonal web. (a) Integer level sets for each of ϕ_1, ϕ_2, ϕ_3 and true geodesics for comparison. (b) Flattening of the surface by the mapping $\psi(\mathbf{x}) = (\phi_1(\mathbf{x}), (\phi_1(\mathbf{x}) + 2\phi_2(\mathbf{x}))/\sqrt{3})$. (c)–(d): Using ψ as texture mapping, patterns with hexagonal combinatorics can be transferred to the surface. (e) Detail of a geometric pattern inspired by Islamic art. Long and thin components follow geodesic curves on the surface and can therefore be manufactured by bending of wooden panels.

The linear systems to be solved in each round of iteration are sparse, since the single terms which contribute to (6) involve only local differential operators which are defined in terms of small vertex neighborhoods. For sparse Cholesky factorization we employ CHOLMOD [Chen et al. 2008].

5 Geodesic webs

Timber constructions like the one of Figure 4 follow a curve pattern with regular combinatorics. For manufacturing and statics reasons, one would like these guiding curves to be geodesics. Questions of this kind immediately lead us to the investigation of systems of curves on surfaces with both geometric and topological properties. The most important concept here is the *hexagonal web*, which means 3 families of curves which can be continuously mapped to 3 families of parallel straight lines in the plane, as shown by Fig 11b. By selecting a discrete sample of curves from the web we can generate a variety of patterns – see Figures 1 (right), 4, and 11. The condition that families of curves form a hexagonal web is of a topological nature and belongs to the so-called *geometry of webs* [Blaschke and Bol 1938; Chern 1982]. Neglecting some details concerning the domain where a web is defined, we quote a result:

THEOREM 2. *A complete hexagonal web of straight lines in the plane consists of the tangents of an algebraic curve of class 3 (possibly reducible); any class 3 curve yields a hexagonal web [Graf and Sauer 1924]. The variety of geodesic hexagonal webs in a surface is the same as in the plane* $\iff$ *the surface has constant Gaussian curvature [Mayrhofer 1931].*

In summary this means that there is a 9-parameter family of possible hexagonal webs made from geodesics, if the surface under consideration is the plane, or its Gaussian curvature K is constant (see Fig. 12). Note that such surfaces possess mappings into the plane where geodesics become straight lines; such surfaces carry one of the non-Euclidean geometries if $K \neq 0$.

Little seems to be known about surfaces which carry a smaller variety of hexagonal webs made from geodesics. Anyway, for our applications it is more important to have a computational tool for generating a hexagonal web whose curves are *as geodesic as possible*. The level set approach is well suited for that. We describe the three families of curves as level sets of functions ϕ_1, ϕ_2, ϕ_3 with

$$\phi_1 + \phi_2 + \phi_3 = 0. \tag{7}$$

This equation results in a hexagonal web: Mapping the surface S into the plane via $\mathbf{x} \mapsto (\phi_1(\mathbf{x}), \phi_2(\mathbf{x}))$ maps the level sets of ϕ_1 and ϕ_2 to lines $x = \text{const.}$ and $y = \text{const.}$, resp., while the level sets of ϕ_3 are mapped to the lines $x + y = \text{const.}$ Equation (7) is known in the theory of webs; in fact every hexagonal web can be found in this way.

We implement geodesic webs as follows: We consider two functions ϕ_1, ϕ_2 on the given surface S, and optimize them such that the sum of target functionals according to (6), evaluated for ϕ_1, ϕ_2, and $\phi_3 := -\phi_1 - \phi_2$ becomes minimal. For results, see Figure 1 (right) and Figure 11. A different kind of web is shown by Fig. 19.

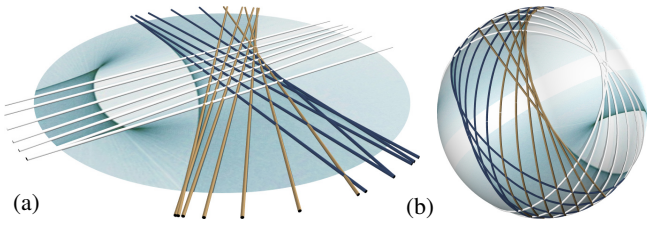

Figure 12: *Hexagonal webs and class 3 curves.* (a) The condition that a straight line $u_0 + u_1 X + u_2 Y = 0$ is in the web reads $\sum_{\substack{i+j+k=3 \\ i,j,k \geq 0}} a_{ijk} u_0^i u_1^j u_2^k = 0$. This equation characterizes the tangents of a class 3 curve, and is determined, up to a factor, by 9 given lines in general position. The colors given to the tangents identify the 3 families of a hexagonal web. (b) A geodesic web on the sphere. It is transformed to a planar one by projection from the center.

6 Global solution of the cladding problem

When the input surface is more complicated, it is harder to cover it with a single geodesic pattern. We have already encountered such difficulties in Section 3 where we discussed the evolution of a geodesic curve. We saw that the Gaussian curvature of the input surface is responsible for the maximal length of a strip which is bounded by geodesic curves. We are thus led to the question of *segmentation* of the input surface such that each piece can be covered by a geodesic 1-pattern.

For this purpose we employ a device not used in previous sections, namely *geodesic vector fields* and *piecewise-geodesic vector fields*. This section describes a general setup related to geodesic vector fields, shows how to interactively design a near-geodesic vector field by means of a certain reduced eigenbasis of fields, and demonstrates how to subsequently modify (*sharpen*) it to make it

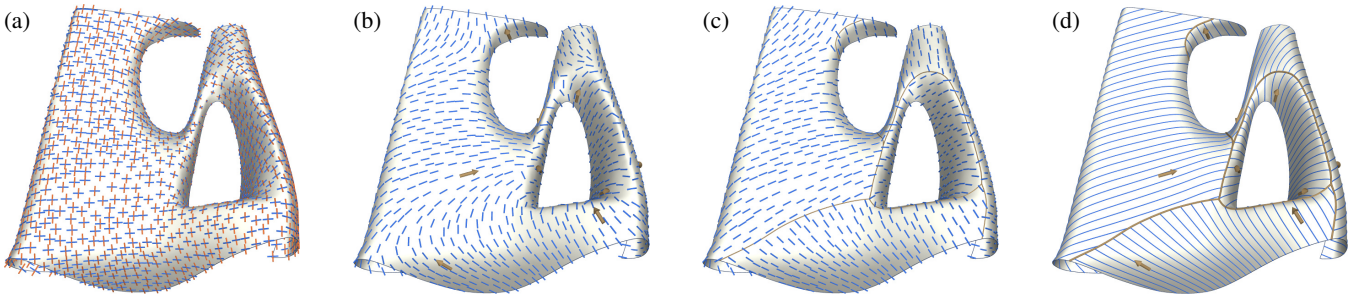

Figure 13: *Processing pipeline for the global cladding problem.* (a) The first two elements of the reduced basis which spans the vector field design space. (b) User's selection $\mathbf{v}^*_{f_1}, \mathbf{v}^*_{f_2}, \ldots$ indicated by arrows, and blue design vector field $\mathbf{v}^\circ$ adapted to this selection. (c) Sharpened vector field $\mathbf{v}$ which is now piecewise geodesic together with the boundaries of macro patches which lie where the vector field is sharp. (d) Segmentation into finitely many geodesic 1-patterns which are aligned with the user's selection. This surface is taken from the interior facade of the *Heydar Aliev Merkezi Project* by Zaha Hadid Architects.

piecewise geodesic. Finally, we perform segmentation of the input surface along the curves where the resulting vector field is sharp. To find the actual geodesic curves defined by the vector field, we refer back to the level set method of Section 4.

Geodesic vector fields. A vector field $\mathbf{v}$ on a surface S is *geodesic* if it consists of tangent vectors of a 1-parameter family of geodesic curves covering S. Later we also encounter piecewise-geodesic fields which fulfill the geodesic property in the inside of certain patches. The following characterization of the geodesic property employs the notation $\nabla_{\mathbf{x}}(\mathbf{v})$, which means the *covariant derivative* of a vector field $\mathbf{v}$ in direction of the tangent vector $\mathbf{x}$, and which is defined as the tangential component of the ordinary directional derivative [do Carmo 1976].

PROPOSITION 3. *A vector field $\mathbf{v}$ of constant length is geodesic $\iff$ for all points of the surface, the linear mapping $\mathbf{x} \mapsto \nabla_{\mathbf{x}}(\mathbf{v})$ in the tangent plane is symmetric.*

Proof: $\|\mathbf{v}\| = \text{const.}$ implies that $\nabla_{\mathbf{x}}(\mathbf{v})$ is orthogonal to $\mathbf{v}$, for all $\mathbf{x}$. The geodesic condition is $\nabla_{\mathbf{v}}(\mathbf{v}) = 0$ everywhere. Among the linear mappings which map the entire tangent plane to $\mathbf{v}^\perp$, the symmetric ones are exactly those which map $\mathbf{v}$ to zero. □

Implementing geodesic vector fields. In our implementation, the surface S is represented as a triangle mesh (V, E, F). The vector field is represented by unit vectors $\mathbf{v}_f$ attached to the incenters $\mathbf{m}_f$ of faces $f \in F$. Consider two adjacent faces f_1, f_2, such that the face f_2 has been unfolded into the plane of f_1 (in the following text, the unfolded positions of items associated with f_2 are marked with a hat). In order to capture the condition of Prop. 3, we endow each face with a local coordinate system and a Jacobi matrix J_f such that

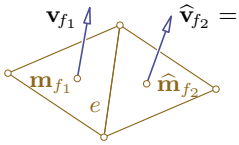

$$\widehat{\mathbf{v}}_{f_2} = \mathbf{v}_{f_1} + J_{f_1} \cdot (\widehat{\mathbf{m}}_{f_2} - \mathbf{m}_{f_1}) + \mathbf{r}_e, \quad \text{where } J_f = \begin{pmatrix} g_{1,f} & g_{2,f} \\ g_{2,f} & g_{3,f} \end{pmatrix}. \tag{8}$$

Here $\mathbf{r}_e$ is a remainder term associated with the edge $e = f_1 \cap f_2$.

This manner of discretizing the symmetry of the covariant derivative – as postulated by Prop. 3 – comes from two facts: (i) covariant differentiation is invariant if an isometric deformation is applied, so we may unfold the neighboring triangles into the plane of the triangle under consideration; (ii) in a plane, $\nabla_{\mathbf{x}}(\mathbf{v})$ equals the ordinary directional derivative of $\mathbf{v}$ w.r.t. the vector $\mathbf{x}$, i.e., it equals multiplication of a Jacobi matrix with $\mathbf{x}$. The condition of Prop. 3 now means symmetry of the Jacobi matrix.

In summary, the vector field $\mathbf{v} = (\mathbf{v}_f)_{f \in F}$ is a geodesic vector field, if its length $\|\mathbf{v}_f\|$ is constant for all faces f, and we can find a collection of coefficients $\mathbf{g} = (\mathbf{g}_f)_{f \in F}$ with $\mathbf{g}_f = (g_{1,f}, g_{2,f}, g_{3,f})$, such that (8) holds with the $\mathbf{r}$'s below some threshold.

The following functional attempts to quantify how well $\mathbf{v}$ satisfies the geodesic property. It will turn out to be very useful for the next task (interactive editing of geodesic vector fields). We let

$$Q(\mathbf{v}) = \min_{\mathbf{g} \in \mathbb{R}^{3|F|}} \Big(\sum_{e \in E} w_e \|\mathbf{r}_e(\mathbf{v}, \mathbf{g})\|^2 + \lambda_r \|\mathbf{g}\|^2 \Big). \tag{9}$$

The term including λ_r is for regularization; we choose the factor λ_r proportional to a characteristic edge length in the mesh. The edge weights $w_e \geq 0$ are for downweighting areas where we do not care about the geodesic property and where we (later) want to encourage formation of a patch boundary. We chose to downweight areas of high curvature; so we let $w_e = \exp(-\kappa_e^2 / 2\mu^2)$, where κ_e is the normal curvature across the edge e, and μ is computed as a median of all absolute values $|\kappa_e|$. We say that these weights are median-weights w.r.t. the mapping $e \mapsto |\kappa_e|$.

Since the $\mathbf{r}_e$'s which contribute to the value $Q(\mathbf{v})$ depend only on $\mathbf{v}$, we can also write $\mathbf{r}_e(\mathbf{v})$. The following turns out to be important:

PROPOSITION 4. *There is a positive semidefinite symmetric matrix H, which depends on the given mesh, such that $Q(\mathbf{v}) = \mathbf{v}^T H \mathbf{v}$.*

Proof: The bracket expression in (9) has the general form $\mathbf{g}^T A \mathbf{g} + 2\mathbf{g}^T B \mathbf{v} + \mathbf{v}^T C \mathbf{v}$ with symmetric $A, B, C \implies$ its minimum is attained for $\mathbf{g} = -A^{-1} B \mathbf{v}$, so $Q(\mathbf{v}) = \mathbf{v}^T (C - B A^{-1} B) \mathbf{v}$. Positivity is obvious from $Q(\mathbf{v}) \geq 0$. □

Interactive vector field selection. We show how the user can interactively design a piecewise geodesic vector field, by prescribing the values

$$\mathbf{v}^*_{f_1}, \ldots, \mathbf{v}^*_{f_k} \tag{10}$$

of that field in user-selected faces $f_1, \ldots, f_k$. This procedure, which is described in the following paragraphs and which is motivated by [Huang et al. 2009], first amounts to choosing a vector field $\mathbf{v}^\circ$ which is not exactly geodesic but has a reasonably small value of $Q(\mathbf{v}^\circ)$. In a subsequent step $\mathbf{v}^\circ$ is sharpened so as to become a piecewise geodesic vector field $\mathbf{v}$.

In order to achieve interactive editing rates, we precompute a reduced basis $\mathbf{v}^{(1)}, \ldots, \mathbf{v}^{(n)}$ of vector fields and and try to realize the user's selection by a linear combination

$$\mathbf{v}^\circ = x_1 \mathbf{v}^{(1)} + \cdots + x_n \mathbf{v}^{(n)}.$$

of these eigenvectors alone. Our choice is to take the first n eigenvectors of the quadratic form Q (i.e., eigenvectors of the matrix H as defined in Prop. 4). In order to determine $x_1, \ldots, x_n$ and to reinforce the condition $\|\mathbf{v}_f^\circ\| = 1$ which is not satisfied by the eigenvectors, we employ two steps in an alternating way: (i) we let $\bar{\mathbf{v}}_f^\circ = \mathbf{v}_f^\circ / \|\mathbf{v}_f^\circ\|$, and (ii) we determine $x_1, \ldots, x_n$ such that

$$F_{prox} = \sum_{i=1}^{k} \|\mathbf{v}_{f_i}^\circ - \mathbf{v}_{f_i}^*\|^2 + \lambda_r \|\mathbf{v}^\circ\|^2 + \lambda_n \sum_{f \in F} \|\mathbf{v}_f^\circ - \bar{\mathbf{v}}_f^\circ\|^2 \to \min.$$

The weights λ_n, λ_r govern the influence of normalization and regularization terms. The choice of these values is not critical; we used $\lambda_n = 0.1$ and $\lambda_r = 0.01$. We initialize this iteration by letting $\lambda_n = 0$ in the first round. Each round amounts to solving a linear system and a matrix-vector multiplication, and takes $O(n^3) + O(n \cdot |F|)$ time. For instance, with $n = 60$ and $|F| = 40\,000$ we experienced 10 ms per round on a 2 GHz PC. Further, we found 3–5 rounds to be sufficient. Thus, vector field selection can be performed in real time.

Remark 2. The number n determines the degrees of freedom offered to the user; we found $n \approx 50$ to work well. Guidance is given by the magnitude of the first n eigenvalues which should be small, and by the complexity of the object under consideration. Choosing the first eigenvectors of Q to span our design space amounts to choosing a design space where $Q(\mathbf{v}^\circ)$ has small values under the 'wrong' and geometrically meaningless normalization constraint $\|\mathbf{v}^\circ\|^2 = 1$. As all vector fields undergo further treatment anyway, this wrong normalization does not matter. Our purpose was to find a design space which contains enough degrees of freedom, and which is taken from the *low frequency* end of the spectrum (thus avoiding unreasonably small patch sizes).

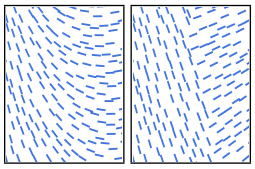

Figure 14: Sharpening a vector field (left) such that it becomes piecewise geodesic (right). This is a detail of Fig. 13.

Vector field sharpening. Segmentation of the given surface S into patches is based on *piecewise geodesic* vector fields, which fulfill the geodesic property in the inside of certain patches (i.e., $\mathbf{r}_e$ is small there), but we allow high values of $\|\mathbf{r}_e\|$ along the patch boundaries. We assume that a vector field $\mathbf{v}^\circ$ is given, and we wish to find another vector field $\mathbf{v}$ which is close to $\mathbf{v}^\circ$, but is piecewise geodesic. We set up an optimization problem as follows:

$$F(\mathbf{v}, \mathbf{g}) = \lambda_v F_{dist}(\mathbf{v}) + \lambda_r \|\mathbf{g}\|^2 + F_{geod}(\mathbf{v}, \mathbf{g}) \to \min, \quad (11)$$

$$F_{geod}(\mathbf{v}, \mathbf{g}) = \sum_{e \in E} w_e \rho(\|\mathbf{r}_e(\mathbf{v}, \mathbf{g})\|), \quad \rho(x) = \frac{x^2}{1 + \alpha x^2}, \quad (12)$$

$$F_{dist}(\mathbf{v}) = \sum_{f \in F} w_f \|\mathbf{v}_f - \mathbf{v}_f^\circ\|^2. \quad (13)$$

The function ρ could be any of the heavy-tailed functions used for image sharpening (see for instance [Levin et al. 2007]). Its purpose is to push the deviations to accumulation areas. We used the robust estimator of Geman and McClure [1987], with $\alpha = 100$ in all examples. Global weights λ_r, λ_v which govern the influence of the regularization term and the proximity of $\mathbf{v}$ to $\mathbf{v}^\circ$ have to be set according to the application. We maintain the condition $\|\mathbf{v}_f\| = 1$, so the variables in this optimization are, besides $\mathbf{g} \in \mathbb{R}^{3|F|}$, the collection of angles θ_f which define the vector $\mathbf{v}_f$ in the local coordinate system of the face f. The optimization problem is solved in the same way as that of Section 4.

The face weights w_f offer the possibility to keep $\mathbf{v}$ close to $\mathbf{v}^\circ$ where $\mathbf{v}^\circ$ already is a geodesic vector field – indicated by smallness of $\mathbf{r}_e(\mathbf{v}^\circ)$. We employ median-weighting w.r.t. the mapping $f \mapsto \sum_{e \in \partial f} \|\mathbf{r}_e(\mathbf{v}^\circ)\|$.

Surface segmentation and pattern layout. Having found a piecewise geodesic vector field $\mathbf{v}$, we now define patches by cutting along the edges where $\mathbf{v}$ is sharp. We first collect all edges $e = f_1 \cap f_2$ where the angle between $\mathbf{v}_{f_1}$ and $\mathbf{v}_{f_2}$ is greater than a threshold value α; such edges indicate patch boundary curves (we use $\alpha = 20^\circ$). We then use the method of Pauly et al. [2003] to polish these curves. We omit details since we do not consider segmentation a new result. Segmentation being completed, we end up with patches $P_1, \ldots, P_M$ which we know can be covered by a smooth geodesic vector field. The layout of evenly spaced geodesics within each P_j is done according to Section 4, augmenting the target functional (6) by

$$F_{align}^{(j)} = \lambda_{user} \sum_{i: f_i \in P_j} \langle \nabla\phi(f), \mathbf{v}_{f_i}^* \rangle^2 + \lambda_{sharp} \sum_{f \in P_j} \langle \nabla\phi(f), \mathbf{v}_f \rangle^2.$$

Minimizing $F_{align}^{(j)}$ means that the geodesics occurring as level sets of ϕ are aligned with the sharpened vector field $\mathbf{v}$ and/or with the user's selection $\{\mathbf{v}_{f_i}^*\}$. The corresponding weights λ_{sharp} and λ_{user} have to be set accordingly. Results are shown in Figs. 1, 13, and 15.

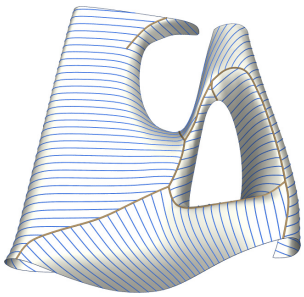

Figure 15: Instead of properly segmenting a surface into parts which can be covered by smooth geodesic 1-patterns, we may look for a weaker solution: cutting it open along curves such that it can be covered by 1-patterns which are smooth everywhere except at the cuts. The present example is almost a true segmentation with only 1 dangling edge.

General remarks. There are several reasons why the interactive procedure of Section 6 is not only nice to have in applications, but is actually necessary: First, the highly nonlinear minimization of the function $F(\mathbf{v}, \mathbf{g})$ in Equation (11) will typically get stuck in local minima, so we cannot expect that unguided minimization of $F(\mathbf{v}, \mathbf{g})$ succeeds. Second, there is a great variety of local minima which cannot clearly be distinguished by the magnitude of $F(\mathbf{v}, \mathbf{g})$ alone. For this reason it is necessary to let the user choose.

7 Discussion

Architectural applications are not limited to timber structures, as the static properties of geodesics apply to any material. An additional bonus is that beams which follow geodesics, being shortest, need less material than other shapes. Fig. 16 shows an example, featuring a 2-pattern of geodesics which is designed for realization in steel rather than in wood.

Comparing the vector field method with other approaches. The segmentation procedure of Section 6 is governed by both user interaction and Gaussian curvature, since it produces patches inside which the Gaussian curvature has a nice behaviour — 'nice' being defined in terms of the capability of being covered with a 1-pattern of geodesic curves. Segmentation of surfaces driven by Gaussian curvature as proposed by [Yamauchi et al. 2005] for even distribution of Gaussian curvature or by [Julius et al. 2005] for near-developable patches probably produces patches which can be covered

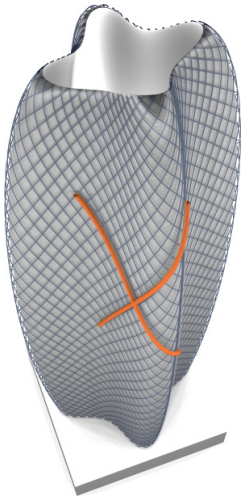

Figure 16: *Relations between families of geodesics.* The level set approach is capable of accommodating additional requirements, such as a desired intersection angle α between the level sets of functions ϕ_1, ϕ_2. This 2-pattern of geodesic curves is imposed on the Warsaw *Lilium Tower* by Zaha Hadid Architects. True geodesics in orange are shown for comparison.

by geodesic 1-patterns. The method of the present paper, however, directly works with geodesics in a user-controlled way; Gaussian curvature is present only implicitly.

This paper contains another way of segmenting a surface into patches which can be covered by almost equidistant geodesics, namely the evolution of broken geodesics as illustrated by Fig. 9 (it even yields a consistent spacing of curves along the patch boundaries). The method of Section 6 is much more flexible, however, and treats each part of the surface in the same way, independent of an initial choice of geodesic to evolve from.

Computation details and timings. For the level set approach, details on the choice of weights, the number of variables, etc., as well as timings are given by Table 1. For the geodesic vector field approach, the choice of weights is detailed by Section 6. Timings are given by Table 2 for three examples, each of which have 40k faces. Preprocessing (eigenspace computation with *Arpack*) needs 30–40 seconds. One round of sharpening takes 1.1 seconds, and the final segmentation needs about 1 second. That table also shows times for the evolution of broken geodesics according to Section 3. Here about 70% of the time is used for the piecewise fitting of curves, the rest is postprocessing like merge, trim, etc.

Fig.	var	iter.	sec	F_κ	F_Δ	F_w	F_{angle}	λ	μ	ν
1	33k	4	32	.25	20			10^{-2}	0	0
10a	10k	10	16	.0006	2470	25		10^{-8}	10^{-4}	0
10b	10k	11	17	.71	392	.0007		10^{-4}	10^{+4}	0
11	21k	12	77	.005	145			10^{-6}	0	0
16	159k	10	419	.66	1050		.26	$3{\cdot}10^{-4}$	0	2.8

Table 1: Details for the level set approach. We show the number of variables, number of iterations, total time for a 3GHz PC, the values of functionals and the weights used in optimization.

Figure	9a	9b	1 (left)	13	17 (left)
seconds	86	113	102	85	73
Method	Evolution		Vector fields		

Table 2: Representative timings for evolution of geodesics, and for the geodesic vector field method. Data apply to a 2GHz PC.

Limitations. Since in a fixed surface the geodesics are only a two-parameter family of curves, often the designer's request cannot be met and one has to compromise (see Fig. 10b for an example of a decision for equal spacing rather than for the geodesic property). This phenomenon can also cause the segmentation process of Section 6 to produce unsatisfactory results, in which case it has to be iterated (see Fig. 17).

Geodesic webs pose many constraints on the involved curves and in fact we cannot expect them even to exist in a mathematically exact way on arbitrary surfaces. Our level set approach produces webs of curves which are as geodesic as possible, but deviations of level curves from true geodesics are inevitable (see Fig. 18). As mentioned in Theorem 2, on constant Gaussian curvature surfaces we have the same variety of geodesic webs as for straight line webs in the plane. This is verified by the fact that the level curves in Figures 11 and 19 are indistinguishable from true geodesics.

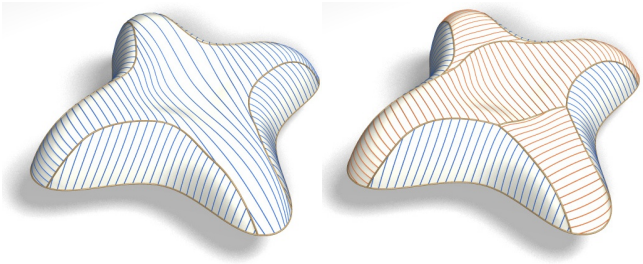

Figure 17: A situation where two rounds of segmentation are necessary because of the unsatisfactory result of the first round.

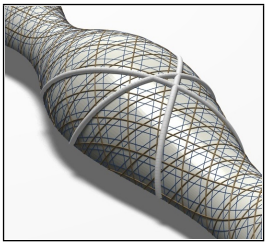

Figure 18: *A hexagonal web of near-geodesics.* We show some curves of the web Fig. 1 is based on. Due to the strong variation in Gaussian curvature they deviate from true geodesics (thick curves).

One major motivation for geodesic patterns is the cladding of freeform surfaces by thin wooden panels. This cladding problem has been considered previously by Pottmann et al. [2008b], in the context of *developable* strips which certainly are a shape which thin panels can assume. In that paper the importance of curve's tangents staying away from asymptotic directions was mentioned. We could incorporate this condition in our level set approach, but we have completely neglected it in this paper. In the negatively curved areas of surfaces, it would very much obstruct our available degrees of freedom. The reason why we chose not to aim at developable strips is that they are not the shape that bent wooden panels assume in general; such panels can be twisted (for other materials, however, this additional aspect has to be observed to a higher degree).

Conclusion and future research. Motivated by problems in freeform architecture we have described three different approaches to the layout and interactive design of geodesic patterns on surfaces. Each of the methods treated in this paper has its specific strength: The Jacobi field approach to the evolution of geodesic curves is best suited to deal with local issues. The level set approach can deal with the global layout of patterns very well, and is efficient in dealing with multiple patterns of geodesic curves which are in some relation, such as the condition that they form a hexagonal 3-web. The vector field approach is capable of solving the global layout and segmentation problem in an interactive way.

This paper seems to be the first where the classical geometry of webs is employed in a geometry processing context. It is likely that

this theory has yet more potential and applications, in particular in architecture.

Acknowledgments. This research has been supported by the Austrian Science Fund (FWF) under grants No. S92-06 and S92-09 (National Science Network *Industrial Geometry*), and by the European Community's 7th Framework Programme under grant agreement 230520 (*ARC*). The authors gratefully acknowledge the support of NSF grants 0808515 and 0914833, of NIH grant GM-072970, and of a joint Stanford-KAUST collaborative grant. We want to express our thanks to Zaha Hadid Architects, London, to be able to work on data which come from some of their current projects.

References

BLASCHKE, W., AND BOL, G. 1938. *Geometrie der Gewebe*. Springer.

CASELLES, V., KIMMEL, R., AND SAPIRO, G. 1997. Geodesic active contours. *Int. J. Comput. Vision 22*, 1, 61–79.

CHEN, J., AND HAN, Y. 1996. Shortest paths on a polyhedron. I. Computing shortest paths. *Int. J. Comput. Geom. Appl. 6*, 127–144.

CHEN, Y., DAVIS, T. A., HAGER, W. W., AND RAJAMANICKAM, S. 2008. Algorithm 887: CHOLMOD, supernodal sparse Cholesky factorization and update/downdate. *ACM Trans. Math. Softw. 35*, 3, #22, 1–14.

CHERN, S. S. 1982. Web geometry. *Bull. Amer. Math. Soc. 6*, 1–8.

DO CARMO, M. 1976. *Differential Geometry of Curves and Surfaces*. Prentice-Hall.

DO CARMO, M. 1992. *Riemannian Geometry*. Birkhäuser.

GEMAN, S., AND MCCLURE, D. E. 1987. Statistical methods for tomographic image reconstruction. *Bull. Inst. Internat. Statist. 52*, 4, 5–21.

GRAF, H., AND SAUER, R. 1924. Über dreifache Geradensysteme. *Sitz. Bayer. Akad. Math.-nat. Abt.*, 119–156.

HUANG, Q., WICKE, M., ADAMS, B., AND GUIBAS, L. 2009. Shape decomposition using modal analysis. *Comput. Graph. Forum 28*, 2, 407–416.

JULIUS, D., KRAEVOY, V., AND SHEFFER, A. 2005. D-charts: Quasi-developable mesh segmentation. *Comput. Graph. Forum 24*, 3, 581–590.

KÄLBERER, F., NIESER, M., AND POLTHIER, K. 2007. QuadCover – surface parameterization using branched coverings. *Comput. Graph. Forum 26*, 3, 375–384.

KIMMEL, R., AND SETHIAN, J. A. 1998. Computing geodesic paths on manifolds. *PNAS 95*, 8431–8435.

LEVIN, A., FERGUS, R., DURAND, F., AND FREEMAN, W. T. 2007. Image and depth from a conventional camera with a coded aperture. *ACM Trans. Graphics 26*, 3, #70, 1–9.

MADSEN, K., NIELSEN, H. B., AND TINGLEFF, O., 2004. Methods for non-linear least squares problems. Lecture Notes. *http://http://www.imm.dtu.dk/courses/02611/nllsq.pdf*.

MAYRHOFER, K. 1931. Sechseckgewebe aus Geodätischen. *Monatsh. Math. Phys. 38*, 401–404.

MÜLLER, H. R. 1941. Über die Striktionslinien von Kurvenscharen. *Monatsh. Math. Phys. 50*, 101–110.

NATTERER, J., BURGER, N., AND MÜLLER, A. 2002. The roof structure "Expodach" at the world exhibition Hannover. In *Proc. 5th Intl. Conf. Space Structures*, 185–193.

OSHER, S. J., AND FEDKIW, R. P. 2002. *Level Set Methods and Dynamic Implicit Surfaces*. Springer Verlag.

PAULY, M., KEISER, R., AND GROSS, M. 2003. Multi-scale feature extraction on point-sampled surfaces. *Comput. Graph. Forum 22*, 3, 281–290.

PIRAZZI, C., AND WEINAND, Y. 2006. Geodesic lines on free-form surfaces: optimized grids for timber rib shells. In *Proc. World Conference on Timber Engineering*. 7pp.

POLTHIER, K., AND SCHMIES, M. 1998. Straightest geodesics on polyhedral surfaces. In *Mathematical Visualization*, Springer, H.-C. Hege and K. Polthier, Eds., 391–409.

POTTMANN, H., HOFER, M., AND KILIAN, A., Eds. 2008. *Advances in Architectural Geometry*. Proc. of Vienna conference.

POTTMANN, H., SCHIFTNER, A., BO, P., SCHMIEDHOFER, H., WANG, W., BALDASSINI, N., AND WALLNER, J. 2008. Freeform surfaces from single curved panels. *ACM Trans. Graphics 27*, 3, #76, 1–10.

SHELDEN, D. 2002. *Digital surface representation and the constructibility of Gehry's architecture*. PhD thesis, M.I.T.

SPUYBROEK, L. 2004. *NOX: Machining Architecture*. Thames & Hudson.

SUTTON, D. 2007. *Islamic Design: A Genius for Geometry*. Walker Publ. Comp.

YAMAUCHI, H., GUMHOLD, S., ZAYER, R., AND SEIDEL, H. P. 2005. Mesh segmentation driven by Gaussian curvature. *Vis. Computer 21*, 659–668.

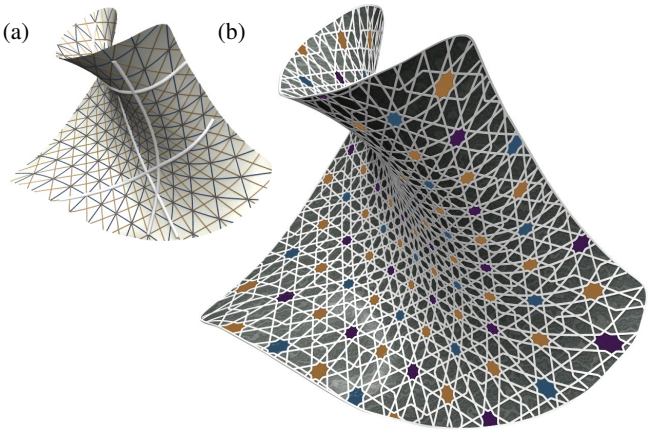

Figure 19: *Geodesic 4-pattern.* For a combination of two hexagonal webs, functions ϕ_1, ϕ_2 are optimized such that level sets of $\phi_1, \phi_2, \phi_1 \pm \phi_2$ are geodesic. (a) Level sets (thin) and true geodesics (thick). Level sets of all four functions are almost truly geodesic, because the Gaussian curvature is nearly constant for this particular surface. (b) Transfer of an Islamic art pattern according to [Sutton 2007] to the surface by the simple texture coordinates $u = \phi_1, v = \phi_2$. The four principal directions in the pattern follow geodesic curves.